Dalton Transactions

RSC Publishing

PAPER

View Article Online
View Journal | View Issue

Electrochemical illumination of thienyl and ferrocenyl chromium(0) Fischer carbene complexes†

Cite this: *Dalton Trans.*, 2013, **42**, 5367

Belinda van der Westhuizen,[a] Pieter J. Swarts,[b] Ian Strydom,[a] David C. Liles,[a] Israel Fernández,[c] Jannie C. Swarts*[b] and Daniela I. Bezuidenhout*[a]

A series of ferrocenyl and thienyl mono- and biscarbene chromium(0) complexes **1–6** were synthesised. The complexes were characterised both spectroscopically and electrochemically, and the single crystal X-ray structure of **3** was determined. Electrochemical measurements in CH_2Cl_2 revealed that the carbene double bond of **1–6** is reduced to an anion radical, $^{-}$Cr–C$^{\cdot}$ at formal reduction potentials <–1.7 V *vs.* FcH/FcH^{+}. A computational study on **1**, **3** and **4** (B3LYP/def2-SVP level) is consistent with electrochemical results in showing that electrochemically generated chromium(I) species may be further electrochemically irreversibly oxidised to chromium(II) at E_{pa} > 0.95 V. The reactivity towards follow-up chemical reactions of the anodically produced Cr(II) species is much higher than the reactivity of the cathodically produced radical anions as the latter was still observably reoxidised to the parent Cr=C species at fast scan rates. The ferrocenyl group is oxidised electrochemically reversibly to ferrocenium at larger potentials than the electrochemically reversible oxidation of the Cr(0) centre to Cr(I). That all redox centres in **1–6** are involved in one-electron transfer steps was confirmed by comparing the ferrocenyl voltammetric wave with those of the other redox centres in linear sweep voltammetric experiments. The ferrocenyl group was electrochemically shown to stabilise the Cr=C centre almost as much as the NHBu, and much more than the ethoxy and thienyl groups.

Received 5th December 2012,
Accepted 4th February 2013

DOI: 10.1039/c3dt32913e

www.rsc.org/dalton

Introduction

The applications of Fischer carbene complexes of the type $[ML_n\{C{=}(XR)R'\}]$ as active or auxiliary ligands in organic synthesis and catalysis evolve around the reactivity of the metal–carbon double bond or the carbene-bonded heteroatom X.[1] Alternatively, modification of conjugated carbene substituents R′ allows for tailored organic synthesis (Fig. 1).

Theoretical calculations have focused on the donor/acceptor nature of the heteroatom X on the carbene substituent,[2] or on the steric and electronic effects of the heteroatom on the carbene ligand.[3] Only a few studies on the use of electrochemistry as an elucidative tool for the abovementioned properties have been reported.[4] In general, electrochemical properties of electro-active compounds, A–R, can be utilised to establish the relative ease by which a redox-active centre, A, may be oxidised (or reduced) in a series of differently R-substituted compounds.[5] The electron-donating or electron-withdrawing properties of different R-groups in a series of compounds may be quantified by relating the formal reduction potential, $E^{o\prime}$, of a redox centre in the compounds with the Gordy scale group electronegativity, χ_R, of R groups of the molecules.[6] Recently, a renewal of interest in the redox behaviour of Group 6 Fischer carbene complexes has been seen.[7] This is a result of their promising application as, for example, electrochemical probes.[8]

In this paper, we report the synthesis, characterisation and results of an electrochemical and computational investigation

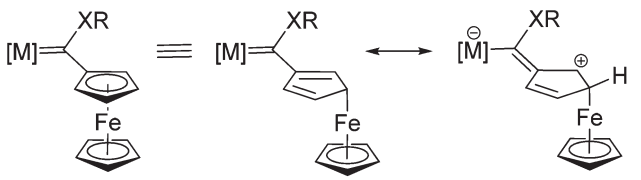

Fig. 1 Two of the many canonical forms that explains the stabilisation of carbenes by a ferrocenyl group.

[a]*Chemistry Department, University of Pretoria, Private Bag X20, Hatfield, 0028, South Africa. E-mail: daniela.bezuidenhout@up.ac.za; Fax: +27-(0)12-420-4687; Tel: +27-(0)12-420-2626*
[b]*Chemistry Department, University of the Free State, PO Box 339, Bloemfontein 9300, South Africa. E-mail: swartsjc@ufs.ac.za; Fax: +27-(0)51-444-6384; Tel: +27-(0)51-401-2781*
[c]*Departamento de Química Orgánica I, Facultad de Química, Universidad Complutense, 28040-Madrid, Spain*

†Electronic supplementary information (ESI) available: The Cartesian coordinates and energies for the optimised compounds **1**, **3** and **4** and the corresponding radical cations. CCDC 913650 for complex **3**. For ESI and crystallographic data in CIF or other electronic format see DOI: 10.1039/c3dt32913e

of 2-thienyl (Th) ethoxy- and two new aminocarbene complexes, as well as the corresponding 2,5-thiendiyl (Th′) biscarbene complexes of chromium(0).[9] The choice of planar, aromatic and electron-rich thiophene as a carbene substituent was based on its ability to be incorporated into the π-delocalised network surrounding the carbene carbon atom, acting as an electron donating substituent for the electrophilic carbene carbon.

In addition, the chromium ferrocenyl (Fc) ethoxycarbene complex $[Cr(CO)_5\{C(OEt)Fc\}]$ (**1**)[10] and the analogous biscarbene complex with bridging 1,1′-ferrocendiyl (Fc′) $[(CO)_5Cr\{C(OEt)(Fc')C(OEt)\}Cr(CO)_5]$ (**2**)[11] were also studied to verify the number of electrons that was transferred in each redox observed. Ferrocene-containing complexes are studied due to the well characterised electrochemical reversible one-electron transfer behaviour of the ferrocenyl group,[12] the ease by which it can be derivatised,[13] and its strong electron-donating properties[14] that may provide significant stabilisation of adjacent electron deficient centres.[15]

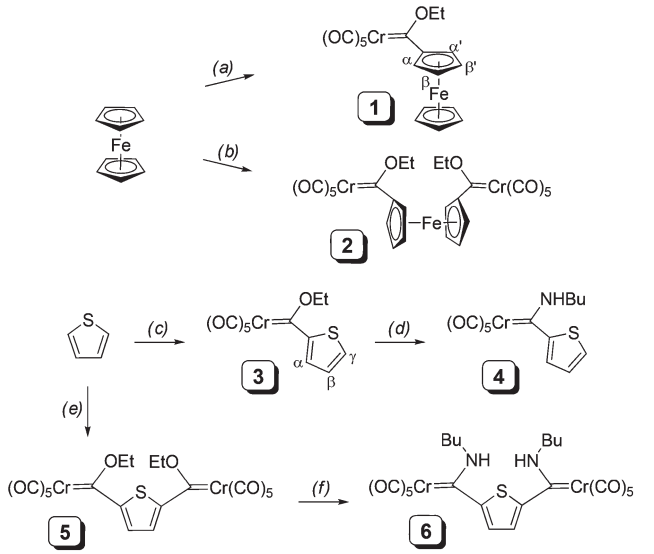

Scheme 1 Reagents and conditions: (a) (i) 1 eq. ^{t}BuLi, thf, −78 °C; (ii) 1 eq. $[Cr(CO)_6]$, thf, −50 °C; (iii) 1.3 eq. Et_3OBF_4, CH_2Cl_2, −30 °C; (b) (i) 2.2 eq. ^{n}BuLi, TMEDA, hexane, 60 °C; (ii) 2 eq. $[Cr(CO)_6]$, thf, −50 °C; (iii) 2.5 eq. Et_3OBF_4, CH_2Cl_2, −30 °C; (c) (i) 1 eq. ^{n}BuLi, thf, −78 °C; (ii) 1 eq. $[Cr(CO)_6]$, thf, −50 °C; (iii) 1.3 eq. Et_3OBF_4, CH_2Cl_2, −30 °C; (d) 1.1 eq. NH_2Bu, Et_2O, rt; (e) (i) 2.2 eq. ^{n}BuLi, thf, −78 °C; (ii) 2 eq. $[Cr(CO)_6]$, thf, −50 °C; (iii) 2.5 eq. Et_3OBF_4, CH_2Cl_2, −30 °C; (f) 2.2 eq. NH_2Bu, Et_2O, rt.

Experimental

General

All operations were carried out under an inert atmosphere of nitrogen or argon gas using standard Schlenk techniques. Solvents were dried by refluxing on sodium metal (hexane, tetrahydrofuran and diethylether) or over phosphorous pentoxide (CH_2Cl_2) and then distilled under nitrogen prior to use. Chemicals were used without further purification unless stated otherwise. Triethyloxonium tetrafluoroborate (Et_3OBF_4) was synthesized according to literature procedures.[16] Purification with column chromatography was done using silica gel 60 (0.0063–0.200 mm) as stationary phase. A Bruker AVANCE 500 spectrometer was used for NMR recordings. ^{1}H NMR spectra were recorded at 500.139 MHz and ^{13}C NMR spectra at 125.75 MHz. The signal of the solvent was used as reference: ^{1}H $CDCl_3$ at 7.24 ppm and ^{13}C $CDCl_3$ at 77.00 ppm. IR spectra were recorded on a Perkin-Elmer Spectrum RXI FT-IR spectrophotometer in hexane as solvent. Only the vibration bands in the carbonyl-stretching region (*ca.* 1600–2200 cm^{-1}) were recorded.

Synthesis of carbene complexes 1–6

Ethoxycarbene complexes **1**,[17] **2**,[11] **3**,[18] and **5**[19] were prepared (Scheme 1) according to published procedures; spectroscopic characterisation data are as follows:

$[Cr(CO)_5\{C(OEt)Fc\}]$ (1). Yield 79%, dark red crystals, NMR ($CDCl_3$) ^{1}H: 4.99 (q, J = 7.1 Hz, 2H, C**H**$_2$), 4.93 (br, 2H, Fc-H$_\alpha$), 4.71 (br, 2H, Fc-H$_\beta$), 4.16 (s, 5H, Fc-Cp), 1.55 (t, J = 7.1 Hz, 3H, C**H**$_3$); ^{13}C: 329.7 (C$_{carbene}$), 223.0 (CO$_{trans}$), 217.3 (CO$_{cis}$), 93.6 (Fc-C$_{ipso}$), 75.5 (O**C**H$_2$), 74.5 (Fc-C$_\alpha$), 72.3 (Fc-C$_\beta$), 70.6 (Fc-Cp), 15.5 (**C**H$_3$). IR ν(CO) (hexane): 2056 m (A″$_1$), 1977 vw (B), 1949 s (A′$_1$), 1938 *vs*. (E).

$[(CO)_5Cr\{C(OEt)(Fc')C(OEt)\}Cr(CO)_5]$ (2). Yield (68%), red-black solid, NMR ($CDCl_3$) ^{1}H: 5.07 (q, J = 7.1 Hz, 4H, C**H**$_2$), 5.00 (dd, J = 2.3, 1.9 Hz, 4H, Fc′-H$_{\alpha,\alpha'}$), 4.73 (dd, J = 2.3, 1.9 Hz, 4H, Fc′-H$_{\beta,\beta'}$), 1.63 (t, J = 7.0, 6H, C**H**$_3$); ^{13}C: 306.2 (C$_{carbene}$), 223.6 (CO$_{trans}$), 217.1 (CO$_{cis}$), 99.2 (Fc′-C$_{ipso}$), 76.2 (Fc′-C$_{\alpha,\alpha'}$), 72.7 (Fc′-C$_{\beta,\beta'}$) 77.4 (**C**H$_2$), 15.5 (**C**H$_3$). IR ν(CO) (hexane): 2054 m (A″$_1$), 1979 sh (B), 1938 *vs*. (A′$_1$ overlap E).

$[Cr(CO)_5\{C(OEt)Th\}]$ (3). Yield (83%), red solid, NMR ($CDCl_3$) ^{1}H: 8.24 (dd, J = 4.1, 0.7 Hz, 1H, Th-H$_\alpha$), 7.68 (dd, J = 5.0, 0.7 Hz, 1H, Th-H$_\gamma$), 7.20 (dd, J = 5.0, 4.1 Hz, 1H, Th-H$_\beta$), 5.17 (q, J = 7.0, 2H, C**H**$_2$), 1.69 (t, J = 7.0, 3H, C**H**$_3$); ^{13}C: 316.4 (C$_{carbene}$), 223.2 (CO$_{trans}$), 217.0 (CO$_{cis}$), 155.4 (Th-C$_{ipso}$), 141.1 (Th-C$_\alpha$), 134.8 (Th-C$_\gamma$), 129.0 (Th-C$_\beta$) 76.0 (**C**H$_2$), 15.2 (**C**H$_3$). IR ν(CO) (hexane): 2058 m (A″$_1$), 1983 vw (B), 1957 s (A′$_1$), 1946 *vs*. (E).

$[(CO)_5Cr\{C(OEt)(Th')C(OEt)\}Cr(CO)_5]$ (5). Yield 75%, purple crystals, NMR ($CDCl_3$) ^{1}H: 8.06 (s, 2H, Th-H$_{\alpha,\alpha'}$), 5.21 (q, 2H, J = 7.2, C**H**$_2$), 1.69 (t, 3H, J = 7.1, C**H**$_3$); ^{13}C: 321.9 (C$_{carbene}$), 223.7 (CO$_{trans}$), 216.5 (CO$_{cis}$), 157.7 (Th′-C$_{ipso}$), 137.1 (Th′-C$_{\alpha,\alpha'}$), 77.4 (**C**H$_2$), 15.2 (**C**H$_3$). IR ν(CO) (hexane): 2054 m (A″$_1$), 1987 vw (B), 1964 s (A′$_1$), 1953 *vs*. (E).

Synthesis of $[Cr(CO)_5\{C(NHBu)Th\}]$ (4). Complex **3** (2 mmol, 0.66 g) was dissolved in ether and *n*-butylamine (2.2 mmol, 0.22 mL) was added at room temperature. A rapid colour change from red to yellow was observed. Volatiles were removed by reduced pressure and column chromatography was performed using a 1 : 1 hexane–CH_2Cl_2 eluent mixture. A duplication of the NMR data sets (^{1}H and ^{13}C) indicates the formation of *syn*- and *anti*-isomers, in a ratio of 1 : 1.3, respectively. Yield 0.63 g (88%), yellow crystals. For *syn*-isomer: NMR ($CDCl_3$) ^{1}H: 8.85 (s, 1H, NH), 7.44 (d, J = 5.0 Hz, 1H, Th-H$_\alpha$), 7.04 (d, J = 3.0 Hz, 1H, Th-H$_\gamma$), 6.80 (d, J = 3.0 Hz, 1H, Th-H$_\beta$), 3.48 (dt, J = 5.0, 4.9 Hz, 2H, NC**H**$_2$), 1.67 (m, 2H, C**H**$_2$CH$_2$), 1.38 (m, 2H, CH$_2$C**H**$_2$), 0.92 (t, J = 7.4 Hz, 3H, C**H**$_3$); For *anti*-

isomer: NMR ($CDCl_3$) ^{1}H: 8.54 (s, 1H, NH), 7.44 (d, J = 5.0 Hz, 1H, Th-H_α), 7.36 (d, J = 3.4 Hz, 1H, Th-H_γ), 7.08 (dd, J = 3.4, 3.0 Hz, 1H, Th-H_β), 4.09 (dt, J = 5.1, 5.0 Hz, 2H, NC**H**$_2$), 1.81 (m, 2H, C**H**$_2$CH$_2$), 1.54 (m, 2H, CH$_2$C**H**$_2$), 1.02 (t, J = 7.3 Hz, 3H, C**H**$_3$); For *syn*-isomer; ^{13}C: 271.9 ($C_{carbene}$), 222.9 (CO_{trans}), 217.1 (CO_{cis}), 148.8 (C_{ipso}), 137.3 (Th-C_α), 127.2 (Th-C_γ), 122.5 (Th-C_β), 51.3 (N**C**H$_2$), 31.6 (**C**H$_2$CH$_2$), 19.6 (CH$_2$**C**H$_2$), 13.5 (**C**H$_3$). For *anti*-isomer; ^{13}C: 260.9 ($C_{carbene}$), 223.1 (CO_{trans}), 217.4 (CO_{cis}), 155.6 (C_{ipso}), 138.5 (Th-C_α), 128.3 (Th-C_γ), 126.7 (Th-C_β), 53.3 (N**C**H$_2$), 31.8 (**C**H$_2$CH$_2$), 20.00 (CH$_2$**C**H$_2$), 13.7 (**C**H$_3$). IR ν(CO) (hexane): 2056 m (A″$_1$), 1977 vw (B), 1918 s (A′$_1$), 1942, 1934 *vs*. (E). Anal. calc. for $CrC_{14}H_{13}NO_5S$: C, 46.79; H, 3.65. Found: C, 47.47; H, 3.87.

Synthesis of [(CO)$_5$Cr{C(NHBu)(Th′)C(NHBu)}] (6). Complex **5** (2 mmol, 1.16 g) was dissolved in ether and *n*-butylamine (4.2 mmol, 0.42 mL) was added at room temperature. The colour changed from purple to deep yellow and volatiles removed under reduced pressure. Column chromatography was performed using a 1 : 1 hexane–CH_2Cl_2 solvent mixture. Yield 0.95 g (75%), dark yellow crystals. A mixture of 3 isomers was obtained, which could not be separated. Significant overlap of the resonances in the ^{1}H NMR spectrum was observed, and the data reported were integrated over the collective region for each chemical shift. The ^{13}C NMR shifts were assigned from 2D NMR experiments and relative intensities, and the *syn*,*syn*-, *anti*,*anti*- and *syn*,*anti*-isomers could be distinguished. NMR ($CDCl_3$) ^{1}H: 8.80, 8.64, 8.50, 8.35 (s, 2H, N**H**), 7.87, 7.84, 7.70, 7.69 (2H, Th-$H_{\alpha,\alpha'}$) 4.13–3.79, 3.58–3.34 (m, 4H, NC**H**$_2$), 1.82–1.55 (m, 4H, C**H**$_2$CH$_2$), 1.40–1.22 (m, 4H, CH$_2$C**H**$_2$), 0.95–0.84 (m, 6H, C**H**$_3$). For *syn*,*syn*-isomer; ^{13}C: 268.8($C_{carbene}$), 223.2 (CO_{trans}), 217.5 (CO_{cis}), 155.2 (C_{ipso}), 133.2 (Th′-$C_{\alpha,\alpha'}$), 53.1 (N**C**H$_2$), 31.6 (**C**H$_2$CH$_2$), 22.7 (CH$_2$**C**H$_2$), 14.1 (**C**H$_3$). For *anti*,*anti*-isomer; ^{13}C: 258.1($C_{carbene}$), 223.0 (CO_{trans}), 217.5 (CO_{cis}), 153.5 (C_{ipso}), 137.8 (Th′-$C_{\alpha,\alpha'}$), 51.3 (N**C**H$_2$), 33.3 (**C**H$_2$CH$_2$), 22.1 (CH$_2$**C**H$_2$), 13.7 (**C**H$_3$ For *syn*,*anti*-isomer; ^{13}C: 261.3, 261.0 ($C_{carbene}$), 222.7, 222.5 (CO_{trans}), 217.2, 217.2 (CO_{cis}), 160.4, 160.4 (C_{ipso}), 137.2, 137.1 (Th′-$C_{\alpha,\alpha'}$), 53.4, 53.3 (N**C**H$_2$), 34.7, 33.6 (**C**H$_2$CH$_2$), 22.2, 22.1 (CH$_2$**C**H$_2$), 13.8, 13.7 (**C**H$_3$). IR ν(CO) (hexane): 2054 m (A″$_1$), 1975 w (B), 1918 s (A′$_1$), 1935 *vs*. (E). Anal. calc. for Cr_2 $C_{24}H_{22}N_2O_{10}S$: C, 45.42; H, 3.50. Found: C, 45.57; H, 3.45.

Crystal structure determination

The crystal data collection and refinement details for complex **3** are summarized in Table 3, and the Ortep/PovRay diagram (Fig. 2).[20] The X-ray crystal structure analysis was performed using data collected at 23 °C on a Bruker kappa duo diffractometer with a PROTON CMOS detector and APEX2 control software[21] using QUAZAR-multilayer-optics-monochromated, Mo-Kα radiation by means of a combination of ϕ and ω scans. Data reduction was performed using SAINT[21] and the intensities were corrected for absorption using SADABS.[21] The structures were solved by direct methods using SHELXTS[22] and refined by full-matrix least squares using SHELXTL[22] and SHELXL-97.[22] In the structure refinements all hydrogen atoms were added in calculated positions and treated as riding on the atom to which they are attached. All non-hydrogen atoms were refined with anisotropic displacement parameters, all isotropic displacement parameters for hydrogen atoms were calculated as $X \times U_{eq.}$ of the atom to which they are attached, X = 1.5 for the methyl hydrogens and 1.2 for all other hydrogens.

Electrochemistry

Cyclic voltammograms (CV's), square wave voltammograms (SW's) and linear sweep voltammograms (LSV's) were recorded on a Princeton Applied Research PARSTAT 2273 voltammograph running PowerSuite (Version 2.58). All experiments were performed in a dry three-electrode cell. A platinum wire was used as auxiliary electrode while a glassy carbon working electrode (surface area 3.14 mm^2) was utilized after polishing on a Buhler polishing mat first with 1 micron and then with 1/4 micron diamond paste. A silver wire was used as pseudo internal reference under an argon atmosphere inside an M Braun Lab Master SP glovebox filled with high purity argon (H_2O and O_2 < 5 ppm). All electrode potentials are reported using the potential of the ferrocene/ferrocenium redox couple [FcH/FcH$^+$] (FcH = (η^5-C_5H_5)$_2$Fe, $E^{o\prime}$ = 0.00 V) as reference.[23] However, decamethyl ferrocene, Fc*, was used as internal standard to prevent signal overlap with the ferrocenyl of **1** and **2**. Decamethylferrocene has a potential of −550 mV *versus* free ferrocene with ΔE = 72 mV and i_{pc}/i_{pa} = 1 under the conditions employed.[24] Analyte solutions (0.5 mmol dm^{-3}) were prepared in dry CH_2Cl_2 in the presence of 0.1 mol dm^{-3} [(^{n}Bu$_4$)N][PF_6]. Analyses were performed at 20 °C. Data were exported to a spread sheet program for manipulation and diagram preparation (Fig. 3–5).

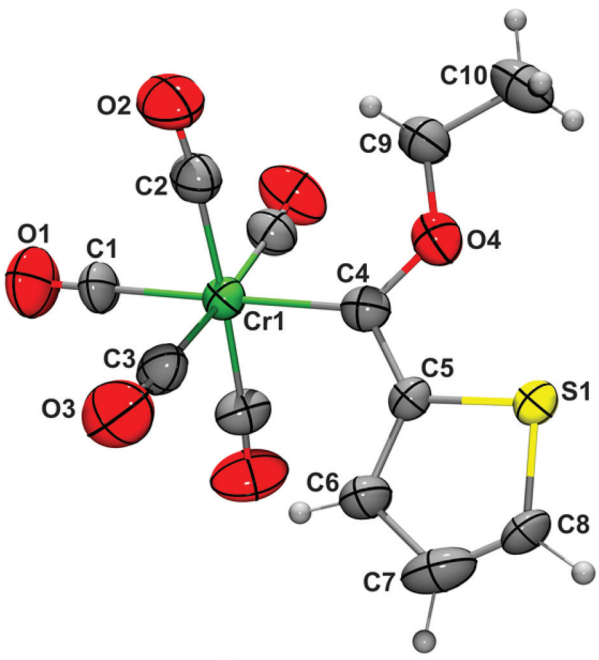

Fig. 2 An Ortep/PovRay[20] drawing of the structure of **3** showing the atom numbering scheme. Only the major orientation of the thienyl-ethoxy-carbene ligand is shown. ADPs are shown at the 50% probability level.

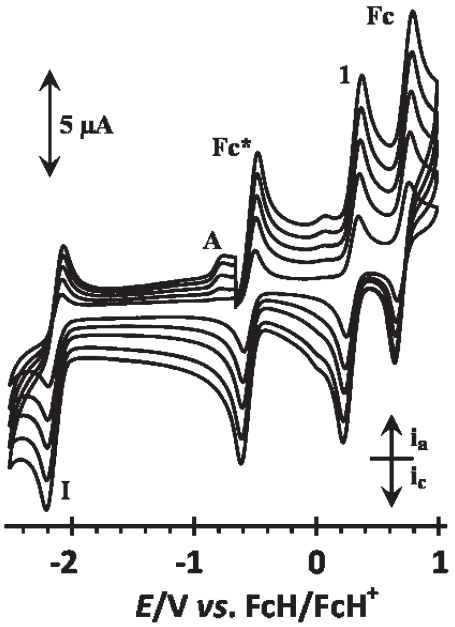

Fig. 3 Cyclic voltammograms of **1** in CH_2Cl_2/0.1 mol dm^{-3} [N(^{n}Bu)$_4$][PF_6] on a glassy carbon-working electrode at scan rates of 100 (smallest currents), 200, 300, 400 and 500 mV s^{-1}. Decamethylferrocene, Fc*, was used as internal standard. Peak A is ascribed to a new species that is generated during Cr=C reduction (peak 1) because if scans are initiated at −1 V, peak A is absent during the initial cycle.

Computational details

Geometry optimizations without symmetry constraints were carried out using the Gaussian09 suite of programs.[25] Electron correlation was partially taken into account using the hybrid functional denoted as B3LYP[26] (and uB3LYP for radical cations) in combination with double-ζ quality plus polarization def-SVP[27] basis set for all atoms (this level is denoted B3LYP/def2-SVP). Calculation of the vibrational frequencies[28] at the optimized geometries showed that the compounds are minima on the potential energy surface.

Results and discussion

Synthesis

Four ethoxycarbene complexes, **1–3**, and **5**, as well as two new aminocarbene complexes **4** and **6** were synthesised according to Scheme 1. The classical Fischer carbene route using Group 6 metal carbonyls was employed for the preparation of the ethoxycarbene complexes **1**, **2**, **3** and **5**: attack of a lithiated substrate on a carbonyl ligand of [$Cr(CO)_6$] forms the metal acylate, which, after alkylation with an oxonium salt, yields the corresponding ethoxycarbene complexes. Synthesis of aminocarbene complexes **4** and **6** were achieved by aminolysis[29] of complexes **3** and **5**, to liberate the new aminocarbene complexes **4** and **6** in 88 and 75% respectively. Compounds were purified by column chromatography to give the products as dark red (ethoxy derivatives) or yellow solids.

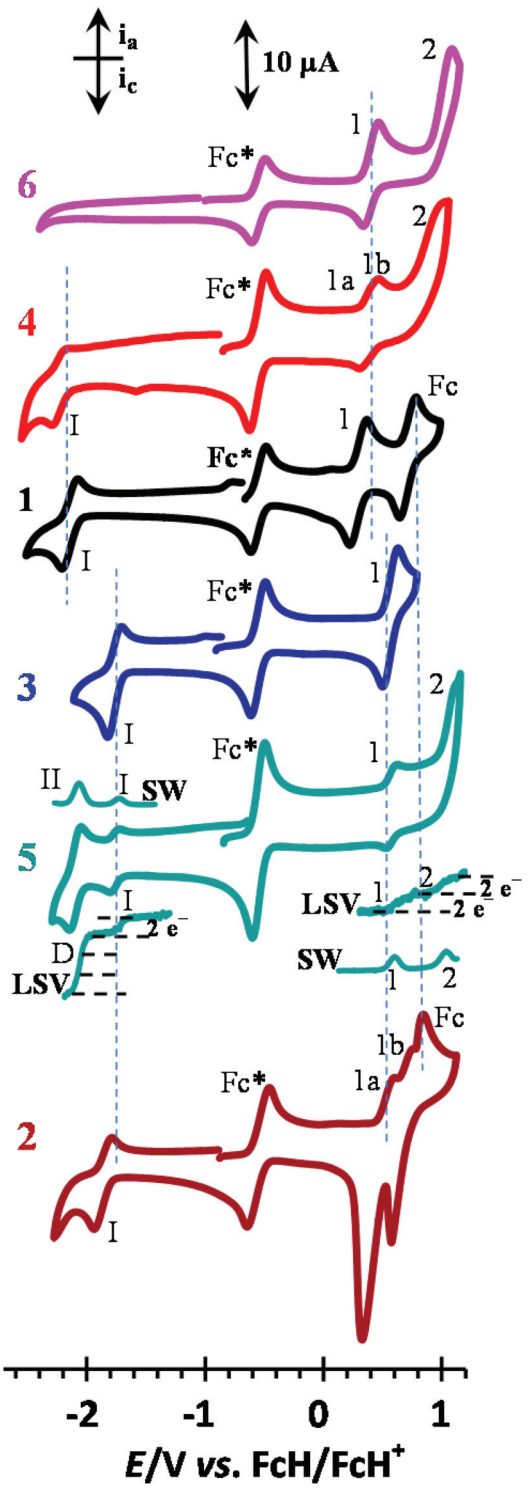

Fig. 4 Cyclic voltammograms of 0.5 mmol dm^{-3} solutions of **1–6** in CH_2Cl_2/0.1 mol dm^{-3} [N(^{n}Bu)$_4$][PF_6] on a glassy carbon-working electrode at a scan rate of 400 mV s^{-1}. Decamethylferrocene, Fc*, was used as internal standard. For **5** ([**5**] = 0.25 mmol dm^{-3} for better clarity) linear sweep (LSV, 2 mV s^{-1}; currents are enhanced 5 times for clarity) and square wave voltammograms (SW, 20 Hz; currents are enhanced 2 times) are also shown.

All neat compounds were stable in the absence of oxygen and could be stored for months in the cold under argon.

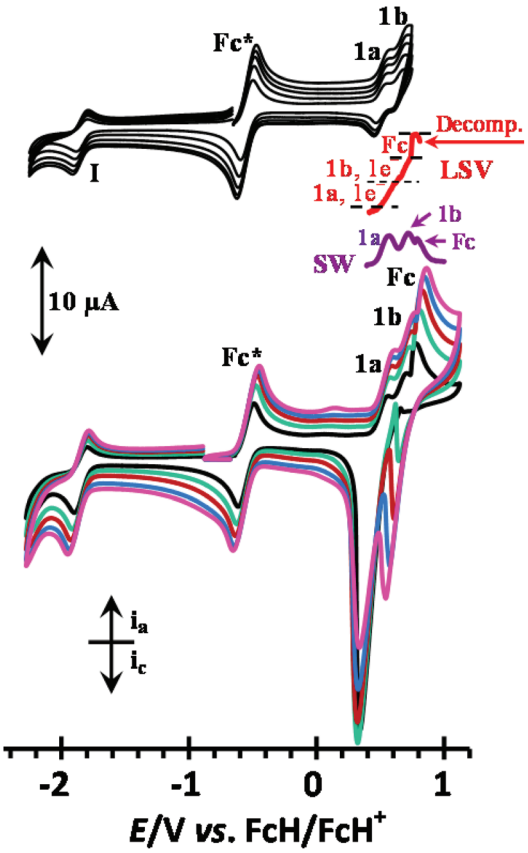

Fig. 5 Bottom: Cyclic voltammograms of **2** in CH_2Cl_2/0.1 mol dm^{-3} $[N(^nBu)_4][PF_6]$ on a glassy carbon-working electrode at scan rates of 100 (smallest currents), 200, 300, 400 and 500 mV s^{-1}. Decamethylferrocene, Fc*, was used as internal standard. Resolved waves **1a** and **1b** are associated with the oxidation of the two Cr(0) species. Top: When the reversal anodic potential is chosen to be sufficiently small to eliminate wave Fc, electrode deposition as indicated by the large cathodic currents in the bottom CV's were not observed. LSV measurements showed waves **1a**, **1b** and Fc are involved in the same number (one) of electrons being transferred.

Electrochemical evidence indicated that in CH_3CN or CH_2Cl_2 solutions, they decomposed to an observable extent within *ca.* 30 minutes. This is slow enough to allow spectroscopic and electrochemical measurements.

Single crystal X-ray structure for 3

The molecular structure of **3** has crystallographic mirror symmetry with the thienyl-ethoxy-carbene ligand, the Cr atom and the carbonyl *trans* to the carbene all lying in the mirror plane.

The carbene ligand is disordered with the two orientations in a ratio of 0.526(8) : 0.474(8), each rotated by 180° from the other about the Cr–$C_{carbene}$ bond. The Cr–$C_{carbene}$ and $C_{carbene}$–O bond distances of 2.077(9) and 1.333(11) Å respectively are comparable to the ranges of Cr–$C_{carbene}$ bond distances, 2.05(1)–2.081(4) Å and $C_{carbene}$–O bond distances, 1.317(5)–1.33(1) Å for a number of chromium-ethoxy-carbene-substituted thienyl structures reported previously.[11,30]

Table 1 Selected ^1H and ^{13}C NMR resonance data and IR ν(CO) stretching frequencies for **1–6**

Complex	H_α δ ^1H (ppm)	$C_{carbene}$ δ ^{13}C (ppm)	A_1'' ν(CO) (cm^{-1})	A_1' ν(CO) (cm^{-1})
1	4.93	329.7	2056	1949
2	5.00	306.2	2054	1938 (overlap E)
3	8.24	316.4	2058	1957
4	7.44, 7.44	271.9, 260.9	2056	1917
5	8.06	321.9	2054	1964
6	7.87, 7.84, 7.70, 7.69	268.8, 261.3, 261.0, 258.1	2054	1918

Spectroscopy

Electronic effects of the carbene substituents can be followed in solution by both NMR and IR spectroscopy. Since H_α (see atom numbering in Scheme 1) is the position closest to the site of coordination of the carbene carbon atom, the chemical shift of this proton is influenced most and is a sensitive probe for electronic ring substituent involvement. Significant downfield shifts of H_α were observed in the ^1H NMR spectra for **1–6** (see Table 1), compared to free ferrocene (4.19 ppm) and thiophene (7.20 ppm). This is consistent with the electron-withdrawing effect of the metal carbonyl fragment bonded to the carbene ligand, comparable, for example, to an ester functionality,[31] as well as the π-delocalization of the (hetero)aryl rings towards stabilizing the electrophilic carbene carbon atom (Fig. 1). Less ring-involvement of the thienyl substituent is seen for both aminocarbene complexes **4** and **6**, as reflected by the higher field H_α resonances. For **4** and **6**, a duplication of all the resonances is also observed in both the ^1H and ^{13}C spectra. This duplication is due to the formation of two different isomers of **4**, rotamers **A** (*anti*-configuration) and **C** (*syn*-configuration) (Scheme 2) with restricted rotation around the $C_{carbene}$–N bond.[32] For **6**, up to three different isomers could be distinguished *via* NMR spectroscopy. These were ascribed to three different biscarbene complex isomers; in one case, a *syn*,*syn*-configuration for both carbene ligands, (*syn*,*syn*-isomer, Experimental section), another where both carbene ligands have *anti*-configuration (*anti*,*anti*-isomer, Experimental section), and finally, the biscarbene complex featuring one carbene ligand with *syn*-, the other ligand with *anti*-configuration (*syn*,*anti*-isomer, Experimental section). The *syn*,*anti*-isomer displays two sets of signals for all observed signals, corresponding to the presence of two different carbene ligands within the molecule. Increased electron donation from the nitrogen lone pair towards the carbene carbon atom results in

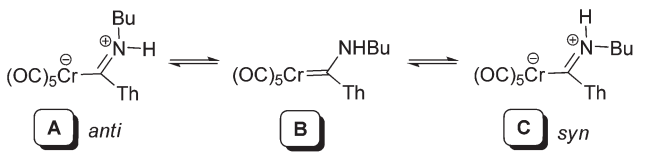

Scheme 2 Stabilisation of aminocarbene complex **B** by formation of the rotameric zwitterionic species **A** and **C**, see text.

a $C_{carbene}$–N bond order greater than one. The bonding situation is best described as an intermediate between the zwitterionic isomers **A**, **C** and the neutral carbene **B**. The carbene carbon resonances obtained from the ^{13}C NMR spectra reflect this marked contribution from the carbene heteroatom substituent, –OEt *vs*. –NHBu. In the case of **4** and **6**, upfield shifts for the carbene carbon atom (271.9, 260.9 ppm for **4**, and 268.8, 261.3, 261.0 and 258.1, respectively, for the three isomers of **6**), compared to **3** and **5** (316.4 and 321.9 ppm, respectively).

The infrared spectra of all complexes clearly displayed the expected band pattern associated with the carbonyl stretches of a $[Cr(CO)_5L]$ system,[33] and no duplication of carbonyl frequencies was observed for the *syn*- and *anti*-isomers of **4** and **6**, as the carbonyls are fairly insensitive to changes of substituents of ligands.[28] In the case of **3**, the IR spectrum measured shows the lifting of the degeneracy of the E-band that appears as two separate signals. In **2**, overlapping of the signals associated with the A'_1 and the E-modes occur. The A''_1 mode defines the symmetric stretch of the CO ligands in the equatorial plane, and is mostly unaffected by the π-acceptor ability of the ligand L; stretching frequencies vary between 2054–2058 cm^{-1} (see Table 1). The A'_1 mode in the pseudo-C_{4v} local symmetry represents the mode with the greatest contribution to the stretching of the C–O bond *trans* to L, and is most affected by changes in the electronic environment caused by the carbene ligand.[29] For aminocarbene complexes **4** and **6**, nitrogen lone pair stabilisation causes a marked decrease in chromium π-backbonding towards the carbene ligand. This is demonstrated by the occurrence of the A'_1-band at lower wavenumbers (Table 1), at frequencies lower than even the E-band.

Electrochemistry and molecular orbital analyses

Cyclic voltammetry (CV), linear sweep voltammetry (LSV), and Osteryoung square-wave voltammetry (SW) were conducted on **1–6** in dry, oxygen-free CH_2Cl_2 utilizing 0.1 mol dm^{-3} $[N(^nBu)_4][PF_6]$ as supporting electrolyte. Data for cyclic voltammetry experiments are summarized in Table 2, CV's are shown in Fig. 3–5.

Four redox processes are identifiable. These are (a) the reduction of the carbene double bond; peaks for this process are labelled I throughout in Fig. 3–5, (b) oxidation of the Cr(0) centre to Cr(I) is observed at peak 1, (c) oxidation of the ferrocenyl group in **1** and **2** (peak Fc), and (d) oxidation of electrochemically generated Cr(I) centre to Cr(II). The latter redox process is labelled as peak 2 in Table 2 and Fig. 4. Molecular orbital calculations (see below) proved peak 2 is associated with the $Cr^{I/II}$ couple and not with oxidation of the :OEt or :NHBu groups.

Central to this electrochemical study is the ferrocenyl oxidation of **1** and **2** (Fig. 3–5). The ferrocenyl group is well established as a moiety that undergoes electrochemical and chemical reversible one electron oxidation. Electrochemical and chemical reversible redox process are characterised by $\Delta E = E_{pa} - E_{pc} = 59$ mV and $i_{pc}/i_{pa} = 1$.[34] For **1**, the ferrocenyl-based redox process is observed at 0.700 V *vs*. the free FcH/FcH^+ couple and exhibits $\Delta E = 89$ mV and $i_{pc}/i_{pa} = 1$ (Table 2). The observed $E^{o\prime} = 0.700$ V is a large shift to positive potentials from 0 V, and illustrates the electrophilic nature of the chromium carbene system.[10] It is important to note that peak 1 in the CV of **1** at $E^{o\prime} = 0.289$ V is not associated with the ferrocenyl couple, but rather with Cr(0) oxidation to Cr(I); this will be discussed below. The ferrocenyl wave of **2** is observed at $E^{o\prime} = 730$ mV, but this redox process leads to adsorption and decomposition, Fig. 4 and 5, implying E_{pc} and current ratios are not reliable. However the LSV applicable to the oxidation of the ferrocenyl group and the two Cr(0) centres (waves 1a, 1b and Fc, Fig. 5) were still consistent with three separate 1-electron transfer processes.

Having confirmed the one-electron transfer nature of the ferrocenyl group in **1**, all the other redox processes in **1–6** can now be interpreted in terms of the number of electrons that is transferred during their redox cycles. Alkene reduction occurs at far negative potentials and in aprotic solvents results in the generation of a radical anion of considerable instability during a one-electron transfer process.[35] Follow-up chemical reactions destroy this electrochemically generated species quickly. Unconjugated alkenes often are reduced at such negative potentials that they cannot be studied in convenient electrochemical solvents; for them reduction often takes place at potentials outside the solvent potential window.[31] Conjugated alkenes are reduced at slightly larger potentials; reduction in aprotic media may be observed in the vicinity of −2 V *vs*. FcH/

Table 2 Cyclic voltammetry data of 0.5 mmol dm^{-3} solutions of **1–6** in CH_2Cl_2 containing 0.1 mol dm^{-3} $[N(^nBu)_4][PF_6]$ as supporting electrolyte at a scan rate of 100 mV s^{-1} and 20 °C. Potentials are relative to the FcH/FcH^+ couple

Complex	Peak no.	$E^{o\prime}$/V, ΔE (mV)	i_{pa} (μA), i_{pc}/i_{pa}
1	I(=)	−2.148, 111	3.20[b], 0.41
	1($Cr^{0/I}$)	0.289, 102	3.48, 0.89
	(Fc)	0.700, 89	3.29, 0.85
	2($Cr^{I/II}$)	—[a], —[a]	—[a], —[a]
2	I(=)	−1.845, 104	3.81[b], 0.39
	1a($Cr^{0/I}$)	0.499, 83	3.71, 0.73
	1b($Cr^{0/I}$)	0.650, 80	3.51, 0.23
	(Fc)	0.730, 97	3.78, <0.1
	2($Cr^{I/II}$)	—[a], —[a]	—[a], —[a]
3	I(=)	−1.762, 98	3.71[b], 0.43
	1($Cr^{0/I}$)	0.565, 85	3.98, 0.88
	2($Cr^{I/II}$)	—[a], —[a]	—[a], —[a]
4	I(=)	−2.232, 132	3.21[b], 0.11
	1a($Cr^{0/I}$)	0.258, 242	1.83, 0.80
	1b($Cr^{0/I}$)	0.435[c], —[c]	1.75, —[c]
	2($Cr^{I/II}$)	0.951[c], —[c]	7.02, —[c]
5	D(=)	−2.091, 88	1.89[b], 0.59
	I(=)	−1.845, 232	0.68[b], 0.78
	1($Cr^{0/I}$)	0.576, 68	0.81, 0.81
	2($Cr^{I/II}$)	1.098[d], —[d]	2.50[d], —[d]
6	I(=)	—[a], —[a]	—[a], —[a]
	1($Cr^{0/I}$)	0.399, 138	4.81, 0.69
	2($Cr^{I/II}$)	1.150[d], —[d]	7.42[d], —[d]

[a] No peak detected within the potential window of the solvent. [b] i_{pc} and i_{pa}/i_{pc} values to maintain the current ratio convention of $i_{forward\ scan}/i_{reverse\ scan}$. [c] Estimated E_{pa}; resolution not good enough to estimate E_{pc}. [d] E_{pa} value, no E_{pc} detected.

Table 3 Crystal, data collection and refinement data for complex **3**

Identification code	BvdWCrThOEt	
Chemical formula	$C_{12}H_8CrO_6S$	
Formula weight	332.25	
Temperature	296(2) K	
Wavelength	0.71073 Å	
Crystal size	0.118 × 0.177 × 0.179 mm	
Crystal habit	Dark orange hexagonal-prism	
Crystal system	Monoclinic	
Space group	$P2_1/m$	
Unit cell dimensions	a = 9.5803(6) Å	α = 90°
	b = 7.6532(5) Å	β = 98.737(3)°
	c = 9.6551(6) Å	γ = 90°
Volume	699.70(8) Å^3	
Z	4	
Density (calculated)	1.577 g cm^{-3}	
Absorption coefficient	0.986 mm^{-1}	
F(000)	336	
Theta range for data collection	2.13 to 26.13°	
Index ranges	$-11 \le h \le 11$, $-9 \le k \le 9$, $-11 \le l \le 11$	
Reflections collected	20 399	
Independent reflections	1497 [R_{int} = 0.0433]	
Completeness to θ = 26.13°	99.8%	
Absorption correction	Multi-scan	
T_{min}, T_{max}	0.677, 0.745	
Structure solution technique	Direct methods	
Structure solution program	*SHELXS*-97	
Refinement method	Full-matrix least-squares on F^2	
Refinement program	*SHELXL*-97	
Function minimized	$\Sigma w(F_o^2 - F_c^2)^2$	
Data/restraints/parameters	1497/0/122	
Goodness-of-fit on F^2	1.199	
Δ/σ_{max}	0.000	
Final R indices all data	R_1 = 0.0861, wR_2 = 0.2371	
1330 data; $I > 2\sigma(I)$	R_1 = 0.0787, wR_2 = 0.2325	
Weighting scheme	$w = 1/[\sigma^2(F_o^2) + (0.0878P)^2 + 3.5878P]$ where $P = (F_o^2 + 2F_c^2)/3$	
Largest diff. peak and hole	0.850 and −0.570 eÅ^{-3}	
R.M.S. deviation from mean	0.122 eÅ^{-3}	

FcH^+.[31] The carbene double bond, Cr=C, of the present series of compounds benefits from the presence of the electron-donating thienyl or ferrocenyl group which allows for conjugation (Fig. 1). Reduction of the Cr=C double bond in **1–5** was observed at potentials less than −1.76 V *vs.* FcH/FcH^+ (Table 2, wave I). That the Cr=C double bond reduction represents a one-electron reduction follows from comparing the i_{pc} value of peak I of **1** (Table 2 and Fig. 3) with the i_{pa} value of the ferrocenyl, *i.e.* wave Fc. Since they are striving to the same value (*ca.* 3.34 μA), and since the ferrocenyl couple represents a one-electron transfer process, wave I must also represent a one-electron reduction process to initially generate $^-$Cr–C$^\cdot$, not only in **1**, but also in the other carbene complexes of this study. This assignment is possible because it is known that the LUMO is mainly carbene-ligand based,[17] and single electron transfer reactions followed by ESI-MS have also indicated the formation of such $^-$Cr–C$^\cdot$ species.[36] Since the orbitals associated with carbenes are delocalized over metal, carbon, and heteroatom, one can envisage the $^-$Cr–C$^\cdot$ species as being stabilised by distributing charge and radical all over the ligand system.

Cr=C reduction is electrochemically quasi reversible because ΔE for this process is substantially larger than 59 mV (Table 2). It is also only partially chemically reversible because the i_{pa}/i_{pc} current ratios for **1–5** (Table 2) deviate more than 40% from unity. This low current ratio is consistent with the high reactivity that is associated with carbon radicals, here $^-$Cr–C$^\cdot$, as described before.[31] The ferrocenyl group stabilized the Cr=C bond much more towards reduction than the thienyl group as the Cr=C bond of **1** was reduced at a potential 386 mV more negative than the carbene double bond of **3**. Strikingly, stabilisation towards reduction of the Cr=C bond with a ferrocenyl group is almost as effective as stabilisation with an amine because the peak I $E^{\circ\prime}$ value of **4** is only 84 mV more negative than that of **1**, but 470 mV more negative than that of **3** (Table 2).

The biscarbene complexes **2** and **5** exhibited Cr=C reduction at potentials 303 mV more positive than **1**. This move towards higher potentials is consistent with the extended conjugation paths present in the bis-compounds.[31] The CV of the biscarbene complex **5** exhibits two reduction waves labelled I and D (Fig. 4). The first, wave I, is assigned to the simultaneous reduction of both the Cr=C bonds as the LSV (Fig. 4) shows it involves transfer of two electrons, one for each double bond. For reference purposes at this stage it is sufficient to observe peak 1 also represents 2 × 1 e$^-$ transfer processes, 1 e$^-$ for each of the Cr(0) processes. The second reduction wave, wave D, is attributed to electrode processes of decomposition products[31] of **5** because the LSV shows that six electrons in total is associated with this redox process. Complex **2** was too unstable for LSV measurement because of decomposition on LSV timescale at large negative potentials. However, the i_{pc} value of wave I for **2**, if one allows for limited decomposition of the Cr=C double bond, and compares it with the i_{pa} values of waves 1a, 1b and Fc, is consistent with two overlapping one-electron Cr=C reductions. The biscarbene **6** showed no Cr=C reductions (Table 2) within the usable potential window of CH_2Cl_2. This is expected since one NHBu group shifted peak I of **4** at −2.232 V to potentials 470 mV more negative compared to peak I of **3**. This is already almost at the limit of the potential window that CH_2Cl_2 allows. Since **6** possesses two NHBu groups, an additional shift to more negative potentials is expected which would result in wave I not being detectable in the workable potential window of CH_2Cl_2.

Oxidation of the Cr(0) centre itself is associated with peak 1 in Fig. 3–5 and Table 2. Once again, by comparing peak currents of wave 1 and wave Fc for **1** it is clear that Cr(0) oxidation involves a one-electron transfer process to generate Cr(I). To decide whether Cr(0) or ferrocenyl oxidation takes place first, from an electrochemical point of view, comparison of the position of wave 1 in **1** with those of amino carbenes **4** and **6**, Fig. 3, is appropriate. It is clear that Cr oxidation waves are in all three cases in the same potential range. The ferrocenyl group is therefore expected to be associated with the wave at larger potentials, that is wave Fc for **1**. This conclusion is mutually consistent with the result obtained by molecular orbital calculations. Density functional theory (DFT) calculations at the B3LYP/def2-SVP[37] level show that the HOMO of complexes **1**, **3** and **4** is mainly located at the chromium(0) atom (Fig. 6),[2d,38] thus confirming that the first oxidation

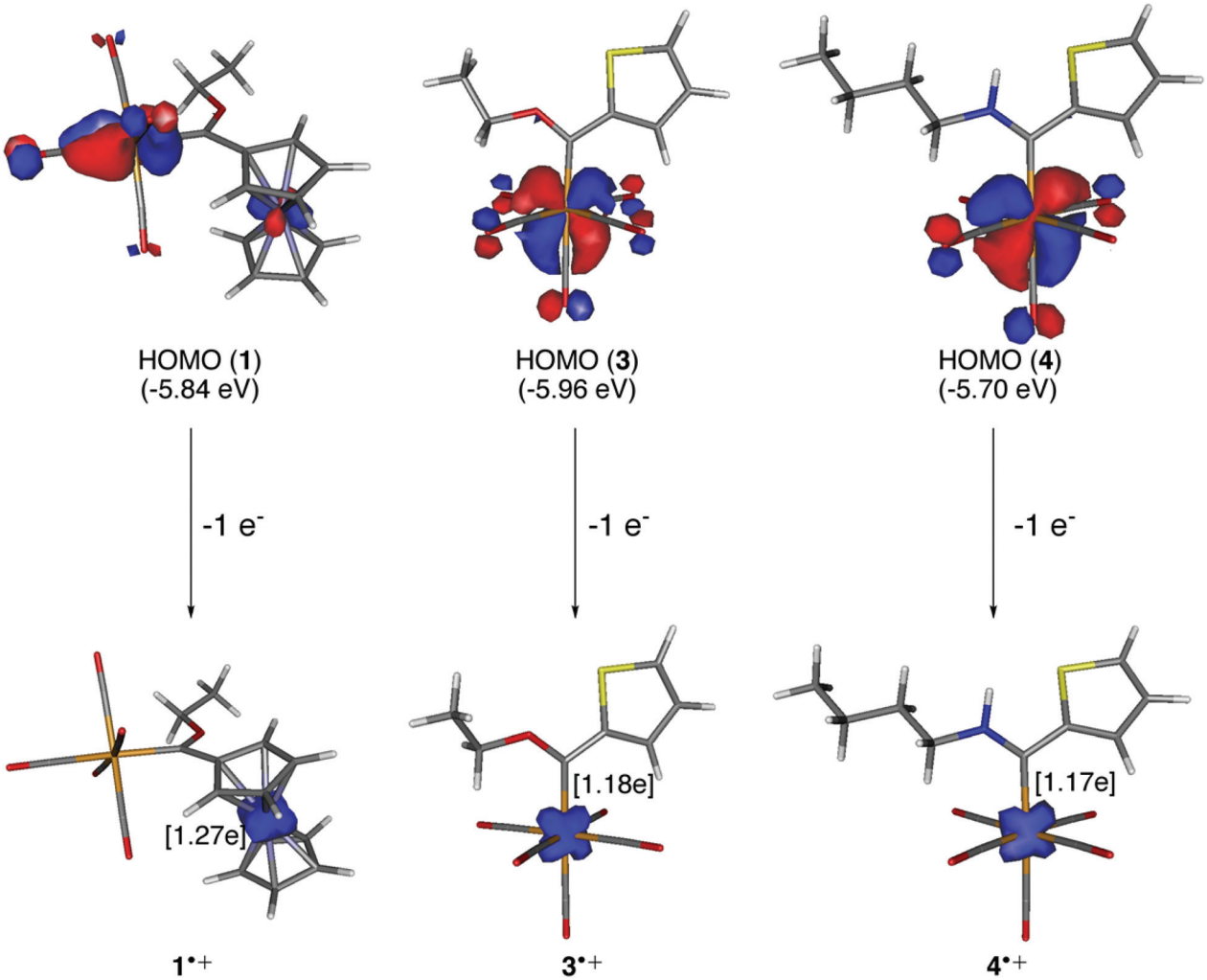

Fig. 6 Computed HOMO's of complexes **1**, **3** and **4** (top) and spin densities of the corresponding radical cations (bottom). Numbers in brackets indicate the computed Mulliken-spin densities. All data have been computed at the B3LYP/def2-SVP level.

process in all complexes can be attributed to the Cr(0) to Cr(I) oxidation. Interestingly, the energy order of the HOMO's (**3** = −5.96 eV > **1** = −5.84 eV > **4** = −5.70 eV, see Fig. 6) agrees with the trend observed in the measured wave 1 electrochemical potentials. Thus, more stabilized HOMO results in a more difficult oxidation process (**3**, $E^{o\prime}$ = 0.565 V > **1**, $E^{o\prime}$ = 0.289 V > **4**, $E^{o\prime}$ = 0.258 V, see Table 2).

Electrochemical evidence also imply that Cr(0) oxidation occurs before ferrocenyl oxidation in the biscarbene complex **2**. Fig. 4, bottom, shows the CV's of **2** where oxidation peaks 1a, 1b and Fc are all three observed. Importantly, each of these waves represents a one-electron transfer process as highlighted by the LSV (Fig. 5). After the third oxidation though (*i.e.* after wave Fc), the complex decomposes on LSV time scale. In contrast, on CV time scale, the observed larger-than-expected peak cathodic currents are consistent with electrode deposition of the oxidised substrate. That electrode deposition takes place after the third (ferrocenyl) oxidation to generate $\mathbf{2}^{3+}$ was confirmed by repeating CV experiments utilising a reversal potential small enough to exclude wave Fc. This resulted in waves 1a and 1b having the normal CV shape. Waves 1a and 1b are associated with two consecutive and partially resolved one-electron Cr(0) oxidations because they are both observed at potentials smaller than the ferrocenyl oxidation of **1**, Table 2. This excludes the possibility of either of these waves to be associated with the oxidation of the ferrocenyl group. After both Cr(0) centres have been oxidised to liberate a more electron-deficient and therefore more electron-withdrawing species, $\mathbf{2}^{2+}$, than the mother compound **2**, the oxidation of the ferrocenyl group of **2** is observed at a larger potential (30 mV larger) than that of **1**. Because the ferrocenyl group is oxidised in a one-electron transfer step, it follows that the Cr(0) centres are also oxidised in a one-electron transfer step as confirmed by LSV measurements. That wave 1 could be resolved into two components 1a and 1b is not unusual. Different formal reduction potentials for symmetrical complexes in which mixed-valent redox-active intermediates are generated (here, for example $\mathbf{2}^{+}$ and $\mathbf{2}^{2+}$ respectively) are well

known in systems that allow through-bond electronic communication between these molecular fragments.[39] Since a similar split of wave 1 into two components was not observed for the thiophene biscarbene derivative **5**, it is concluded that the ferrocenyl group is more effective in allowing through-bond electronic communication between molecular fragments than a thienyl group.

Chromium oxidation in the ethoxy derivatives **1–3** and **5** are, like ferrocenyl oxidation, electrochemical and chemical reversible on CV time scale as ΔE deviated within acceptable limits from the theoretical value of 59 mV and because peak current ratios for these compounds approached unity, Table 2.

The aminobutyl derivatives **4** and **6** exhibit electrochemically irreversible Cr(0) oxidations by virtue of ΔE values exceeding 130 mV under our conditions. Chemical reversibility as identified by peak current ratios approaching 1 is achieved when the reversal anodic potential is small enough to exclude wave 2. The CV of amino carbene **4** hinted that the Cr(0) oxidation peak, peak 1, may also split into two very poorly resolved components, 1a and 1b (Fig. 4). This may be indicative of the presence of two Cr(0) species of sufficient stability and long enough existence time to allow detection on CV timescale. Aminocarbene complexes have high stability due to the existence of the zwitterionic stabilised form as shown in Scheme 2. CV peak 1a is consistent with forms **A** and **C** and peak 1b with form **B**. Although it was possible to distinguish between **A** and **C** spectroscopically, it is unlikely that electrochemical techniques can distinguish between forms **A** and **C** of Scheme 2. Electrochemical observation of two components of a slow equilibrium is not unknown. A similar situation arose with metallocene-containing β-diketones, where the kinetics between keto and enol forms was slow enough to allow detection of both equilibrium components, and to determine the rate of keto to enol conversion and *vice versa*.[40] No evidence of peak 1 splitting into two components could be observed for the biscarbene **6** implying peaks 1a and 1b in this case may simply be so close to each other that they are unresolved.[41]

The last electrochemical process that was observed (peak 2 in Fig. 3 and 4 and Table 2) in **1–6** is the oxidation of the electrochemically generated Cr(I) centre to generate a Cr(II) species (Scheme 3). This electrochemical process is not assigned to oxidation of the :OEt group of **1–3** and **5** or the :NHBu group of **4** and **6** because DFT calculations showed the spin densities of the electrochemically generated radical cations formed during the oxidation of Cr(0) are situated on the newly formed Cr(I) centre and not the hetero atoms (Fig. 6). Cr(I) oxidation of the monocarbenes **1** and **3** fell outside the potential window of the solvent, CH_2Cl_2, but wave 2 in the CV of the bis-complex **5** is consistent with two Cr(I) centres being irreversibly oxidised (Fig. 4) at *ca.* 1.1 V. The LSV suggests that the number of electrons that are transferred at this wave is the same as for wave 1, that is two electrons. In contrast, the CV itself (Fig. 4, Table 2) show $i_{pa,\,wave\,2}$ to be almost double that of $i_{pa,\,wave\,1}$. However, wave 2 is so close to the edge of the potential window of the solvent, that the observed peak anodic current for wave 2 of **5** may well include the beginning of solvent degradation.

The aminocarbene complexes **4** and **6** also exhibit wave 2 (Fig. 3), showing Cr(I) oxidation is irreversible, and occurring at slightly lower potentials than in the ethoxycarbene complexes (Table 2). The irreversible nature of these oxidations illustrates the high reactivity of the Cr(II) species that form during the oxidation. They chemically react to form new species on time scales faster than that of cyclic voltammetry. This contrasts the lower reactivity of the radical anions, $^{-}Cr–C^{\cdot}$, which did not react chemically fast enough to escape detection of electrochemical reoxidation to the mother Cr=C species at fast scan rates (wave I, Fig. 4).

Fig. 6 gathers the computed spin density of the corresponding radical cations formed by one-electron oxidation of complexes **1**, **3**, and **4** to generate $\mathbf{1}^{\cdot+}$, $\mathbf{3}^{\cdot+}$ and $\mathbf{4}^{\cdot+}$. Whereas the unpaired electron is located on the chromium atom in complexes $\mathbf{3}^{\cdot+}$ and $\mathbf{4}^{\cdot+}$, it is located on the iron atom in the ferrocenyl-substituted radical cation $\mathbf{1}^{\cdot+}$. This suggests that the oxidation associated with peak 2 in the CV's of Fig. 4 can be assigned to the oxidation of Cr(I) to Cr(II) in compounds **3** and

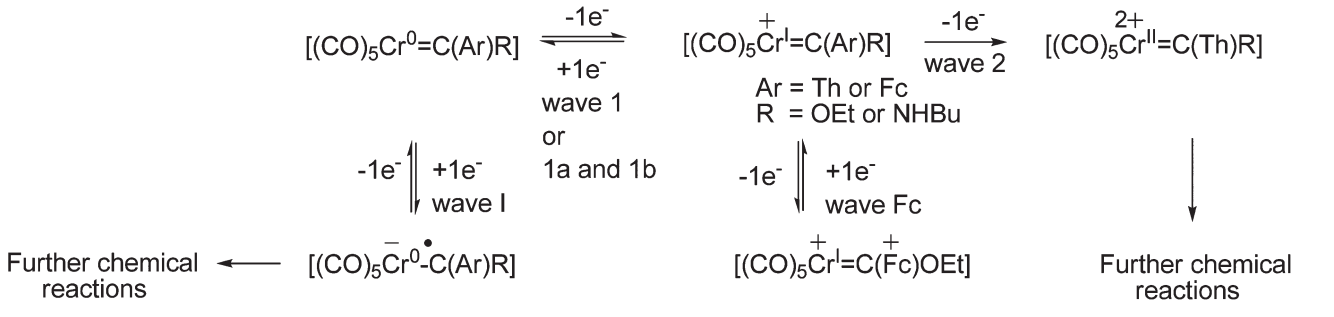

Scheme 3 Electrochemical reactions associated with **1**, **3** and **4**. The radical anions and Cr(II)-containing cations that are generated during the final electrochemical reduction or oxidation step undergoes further chemical reactions. The biscarbene complexes undergo the same reaction sequences except that a second radical anion and Cr(II)-containing cation also forms at potentials close to the edges of the solvent, dichloromethane. Two Cr(0) oxidations was also observed in the biscarbene compounds.

4, while the oxidation associated with wave Fc of complex **1** (Fig. 3) should be a ferrocenyl-based process.

Conclusions

The novel mono- and bisaminocarbene complexes **4** and **6** were prepared by aminolysis of the ethoxy(thienyl) chromium(0) precursors **3** and **5**. Ferrocenyl mono- and bisethoxychromium(0) carbene complexes **1** and **2** were also synthesised and characterised spectroscopically. An electrochemical investigation of these complexes in CH_2Cl_2 showed the carbene double bond, Cr=C, of **1–6** are reduced to an anion radical, $^{-}$Cr–C$^{\cdot}$, at large negative potentials. Electrochemical measurements and DFT calculations were mutually consistent in showing Cr(0) oxidation to Cr(I) occurs before ferrocenyl oxidation, and that the electrochemically generated Cr(I) centre can undergo a second irreversible oxidation to generate Cr(II) at large positive potentials. No oxidation of the heteroatoms in the OEt or NHBu groups could be detected. Cr(II) oxidation for **1** and **3** as well as Cr=C reduction for **6** fell outside the solvent potential window.

The reactivity towards follow-up chemical reactions of the anodically produced Cr(II) centres is much higher than the reactivity of the cathodically produced radical anions as the latter was still observably reoxidised to the parent Cr=C species at fast scan rates. The former showed no indication of any reductive regeneration, even at fast scan rates. The ferrocenyl group is oxidised electrochemically reversible to ferrocenium at larger potentials than the electrochemically reversible oxidation of the Cr(0) centre to Cr(I). All redox active groups in **1–6** were involved in one-electron transfer steps. The ferrocenyl group was electrochemically shown to stabilise the Cr=C centre almost as much as the NHBu, and much more than the ethoxy and thienyl groups. Poorly resolved peak splitting of the Cr(0) oxidation of **4** into components a and b is consistent with the parent aminocarbene being in slow equilibrium with the zwitterionic species [$(OC)_5Cr^{-}$–C=(N^{+}BuH)Th]. An electrochemical scheme is proposed to account for all observed electrochemical steps.

Acknowledgements

This work is supported by the National Research Foundation, (DIB, Grant number 76226; JCS, Grant number 81829). I. F. acknowledges the Spanish MICINN and CAM (Grants CTQ2010-20714-CO2-01/BQU, Consolider-Ingenio 2010, CSD2007-00006, S2009/PPQ-1634).

Notes and references

1 Herndon wrote eleven successive reviews on this topic. The latest one is: J. W. Herndon, *Coord. Chem. Rev.*, 2012, **256**, 1281. To trace the earlier ones, note each review refers in it to the previous one.

2 (*a*) J. Poater, M. Cases, X. Fradera, M. Duran and M. Solà, *Chem. Phys.*, 2003, **294**, 129; (*b*) M. Cases, G. Frenking, M. Duran and M. Solà, *Organometallics*, 2002, **21**, 4182; (*c*) G. Frenking, M. Solà and S. F. Vyboishchikov, *J. Organomet. Chem.*, 2005, **690**, 6178; (*d*) M. L. Lage, I. Fernández, M. J. Mancheno and M. A. Sierra, *Inorg. Chem.*, 2008, **47**, 5253; (*e*) D. A. Valyaev, R. Brousses, N. Lugan, I. Fernández and M. A. Sierra, *Chem.–Eur. J.*, 2011, **17**, 6602; (*f*) N. Lugan, I. Fernández, R. Brousses, D. A. Valyaev, G. Lavigne and N. A. Ustynyukd, *Dalton Trans.*, 2013, **42**, 898.

3 (*a*) I. Fernández, F. P. Cossío, A. Arrieta, B. Lecea, M. J. Mancheño and M. A. Sierra, *Organometallics*, 2004, **23**, 1065; (*b*) D. M. Andrada, M. E. Z. Michoff, I. Fernández, A. M. Granados and M. A. Sierra, *Organometallics*, 2007, **26**, 5854.

4 (*a*) M. K. Lloyd, J. A. McCleverty, D. G. Orchard, J. A. Connor, M. B. Hall, I. H. Hillier, E. M. Jones and G. K. McEwen, *J. Chem. Soc., Dalton Trans.*, 1973, 1743; (*b*) C. P. Casey, L. D. Albin, M. C. Saeman and D. H. Evans, *J. Organomet. Chem.*, 1978, **155**, C37; (*c*) A. Limberg, M. A. N. D. A. Lemos, A. J. L. Pombeiro, S. Maiorana, A. Papagni and E. Licandro, *Port. Electrochim. Acta*, 1995, **13**, 319; (*d*) A. J. L. Pombeiro, *New J. Chem.*, 1997, **21**, 649; (*e*) I. Fernández, M. J. Mancheño, M. Gómez-Gallego and M. A. Sierra, *Org. Lett.*, 2003, **5**, 1237; (*f*) R. Martínez-Álvarez, M. Gómez-Gallego, I. Fernández, M. J. Mancheño and M. A. Sierra, *Organometallics*, 2004, **23**, 4647; (*g*) W. D. Wulff, K. A. Korthals, R. Martínez-Álvarez, M. Gómez-Gallego, I. Fernández and M. A. Sierra, *J. Org. Chem.*, 2005, **70**, 5269; (*h*) M. P. López-Alberca, M. J. Mancheño, I. Fernández, M. Gómez-Gallego, M. A. Sierra, C. Hemmert and K. H. Gornitzka, *Eur. J. Inorg. Chem.*, 2011, 842.

5 (*a*) T. Kuwana, D. E. Bublitz and G. Hoh, *J. Am. Chem. Soc.*, 1960, **82**, 5811; (*b*) T. Ogata, K. Oikawa, T. Fujisawa, S. Motoyama, T. Izumi, A. Kasahara and N. Tanaka, *Bull. Chem. Soc. Jpn.*, 1981, **54**, 3723; (*c*) K.-F. Chin, K.-Y. Wong and C.-M. Che, *J. Chem. Soc., Dalton Trans.*, 1993, 197.

6 (*a*) H. J. Gericke, A. J. Muller and J. C. Swarts, *Inorg. Chem.*, 2012, **51**, 1552; (*b*) A. Auger, A. J. Muller and J. C. Swarts, *Dalton Trans.*, 2007, 3623.

7 (*a*) For a recent review, see: D. I. Bezuidenhout, S. Lotz, D. C. Liles and B. van der Westhuizen, *Coord. Chem. Rev.*, 2012, **256**, 479; (*b*) I. Hoskovcova, R. Zverinova, J. Rohacova, D. Dvorak, T. Tobrman, S. Zalis and J. Ludvik, *Electrochim. Acta*, 2011, **56**, 6853; (*c*) I. Hoskovcova, J. Rohacova, D. Dvorak, T. Tobrman, S. Zalis, R. Zverinova and J. Ludvik, *Electrochim. Acta*, 2010, **55**, 8341; (*d*) A. J. L. Pombeiro, *J. Organomet. Chem.*, 2005, **690**, 6021; (*e*) I. Hoskovcova, J. Rohacova, L. Meca, T. Tobrman, D. Dvorak and J. Ludvik, *Electrochim. Acta*, 2005, **50**, 4911; (*f*) H. G. Raubenheimer, A. du Toit, M. du Toit, J. An, L. van Niekerk, S. Cronje, C. Esterhuysen and A. M. Crouch, *Dalton Trans.*, 2004, 1173.

8 C. Baldoli, P. Cerea, L. Falciola, C. Giannini, F. Licandro, S. Maiorana, P. Mussini and D. Perdiccia, *J. Organomet. Chem.*, 2005, **690**, 5777.
9 While writing this publication, the authors became aware of an independent but simultaneously conducted electrochemical study of related but different chromium carbene complexes, see: R. Metelkova, T. Tobrman, H. Kvapilova, I. Hoskovcova and J. Ludvik, *Electrochim. Acta*, 2012, **82**, 470.
10 J. A. Connor, E. M. Jones and J. P. Lloyd, *J. Organomet. Chem.*, 1970, **24**, C20.
11 D. I. Bezuidenhout, E. van der Watt, D. C. Liles, M. Landman and S. Lotz, *Organometallics*, 2008, **27**, 2447.
12 (*a*) A. Hildebrandt, T. Rüffer, E. Erasmus, J. C. Swarts and H. Lang, *Organometallics*, 2010, **29**, 4900; (*b*) V. Chandrasekhar and R. Thirumoorthi, *Organometallics*, 2007, **26**, 5415; (*c*) S. Ogawa, H. Muroaka, K. Kikuta, F. Saito and R. Sato, *J. Organomet. Chem.*, 2007, **692**, 60.
13 (*a*) W. L. Davis, R. F. Shago, E. H. G. Langner and J. C. Swarts, *Polyhedron*, 2005, **24**, 1611; (*b*) P. J. Swarts, M. Immelman, G. J. Lamprecht, S. E. Greyling and J. C. Swarts, *S. Afr. J. Chem.*, 1997, **50**, 208; (*c*) S. Campidelli, L. Perez, J. Rodrigues-Lopez, J. Barbera, F. Langa and R. Deschenaux, *Tetrahedron*, 2006, **62**, 2115.
14 J. Conradie and J. C. Swarts, *Organometallics*, 2009, **28**, 1018.
15 (*a*) B. Bildstein, *J. Organomet. Chem.*, 2001, **617–618**, 28; (*b*) E. W. Neuse and D. S. Trifan, *J. Am. Chem. Soc.*, 1963, **85**, 1952.
16 H. Meerwin, *Org. Synth.*, 1966, **46**, 113.
17 D. I. Bezuidenhout, W. Barnard, B. van der Westhuizen, E. van der Watt and D. C. Liles, *Dalton Trans.*, 2011, **40**, 6711.
18 J. A. Connor and J. P. Lloyd, *J. Chem. Soc., Dalton Trans.*, 1972, **14**, 1470.
19 Y. M. Terblans, H. M. Roos and S. Lotz, *J. Organomet. Chem.*, 1998, **566**, 133.
20 (*a*) L. J. Faruggia, *J. Appl. Crystallogr.*, 1997, **30**, 565; (*b*) C. J. Cason, *POV-RAY for Windows*, Persistence of Vision, 2004.
21 *APEX2 (including SAINT and SADABS)*, Bruker AXS Inc., Madison, WI, 2012.
22 G. M. Sheldrick, *Acta Crystallogr., Sect A: Foundam. Crystallogr.*, 2008, **64**, 112.
23 (*a*) G. Gritzner and J. Kuta, *Pure Appl. Chem.*, 1984, **56**, 461; (*b*) R. R. Gagne, C. A. Koval and G. C. Lisensky, *Inorg. Chem.*, 1980, **19**, 2855.
24 Leading references describing the electrochemical activity and behaviour of ferrocene and decamethylferrocene in a multitude of organic solvents are (*a*) I. Noviandri, K. N. Brown, D. S. Fleming, P. T. Gulyas, P. A. Lay, A. F. Masters and L. Phillips, *J. Phys. Chem. B*, 1999, **103**, 6713; (*b*) N. G. Connelly and W. E. Geiger, *Chem. Rev.*, 1996, **96**, 877; (*c*) J. Ruiz and D. Astruc, *C. R. Acad. Sci., Ser. IIc: Chim.*, 1998, **1**, 21; (*d*) R. J. Aranzaes, M. C. Daniel and D. Astruc, *Can. J. Chem.*, 2006, **84**, 288.
25 M. J. Frisch, G. W. Trucks, H. B. Schlegel, G. E. Scuseria, M. A. Robb, J. R. Cheeseman, G. Scalmani, V. Barone, B. Mennucci, G. A. Petersson, H. Nakatsuji, M. Caricato, X. Li, H. P. Hratchian, A. F. Izmaylov, J. Bloino, G. Zheng, J. L. Sonnenberg, M. Hada, M. Ehara, K. Toyota, R. Fukuda, J. Hasegawa, M. Ishida, T. Nakajima, Y. Honda, O. Kitao, H. Nakai, T. Vreven, J. A. Montgomery Jr., J. E. Peralta, F. Ogliaro, M. Bearpark, J. J. Heyd, E. Brothers, K. N. Kudin, V. N. Staroverov, R. Kobayashi, J. Normand, K. Raghavachari, A. Rendell, J. C. Burant, S. S. Iyengar, J. Tomasi, M. Cossi, N. Rega, J. M. Millam, M. Klene, J. E. Knox, J. B. Cross, V. Bakken, C. Adamo, J. Jaramillo, R. Gomperts, R. E. Stratmann, O. Yazyev, A. J. Austin, R. Cammi, C. Pomelli, J. W. Ochterski, R. L. Martin, K. Morokuma, V. G. Zakrzewski, G. A. Voth, P. Salvador, J. J. Dannenberg, S. Dapprich, A. D. Daniels, Ö. Farkas, J. B. Foresman, J. V. Ortiz, J. Cioslowski and D. J. Fox, *Gaussian 09, Revision B.1*, Gaussian, Inc., Wallingford, CT, 2009.
26 (*a*) A. D. Becke, *J. Chem. Phys.*, 1993, **98**, 5648; (*b*) C. Lee, W. Yang and R. G. Parr, *Phys. Rev. B: Condens. Matter*, 1998, **37**, 785.
27 F. Weigend and R. Ahlrichs, *Phys. Chem. Chem. Phys.*, 2005, **7**, 3297.
28 J. W. McIver and A. K. Komornicki, *J. Am. Chem. Soc.*, 1972, **94**, 2625.
29 (*a*) D. I. Bezuidenhout, D. C. Liles, P. H. van Rooyen and S. Lotz, *J. Organomet. Chem.*, 2007, **692**, 774; (*b*) U. Klabunde and E. O. Fischer, *J. Am. Chem. Soc.*, 1967, **89**, 7141.
30 (*a*) M. Landman, H. Görls and S. Lotz, *J. Organomet. Chem.*, 2001, **617**, 280; (*b*) M. Landman, H. Görls and S. Lotz, *Eur. J. Inorg. Chem.*, 2001, 233; (*c*) M. Landman, J. Ramontja, M. van Staden, D. I. Bezuidenhout, P. H. van Rooyen, D. C. Liles and S. Lotz, *Inorg. Chim. Acta*, 2010, **363**, 705.
31 T. E. Pickett and C. J. Richards, *Tetrahedron Lett.*, 1999, **40**, 5251.
32 (*a*) E. W. Post and K. L. Watters, *Inorg. Chim. Acta*, 1978, **26**, 29; (*b*) E. Moser and E. O. Fischer, *J. Organomet. Chem.*, 1968, **15**, 147.
33 (*a*) P. S. Braterman, *Metal Carbonyl Spectra*, Academic Press Inc., London, 1975, p. 68; (*b*) D. M. Adams, *Metal–Ligand and Related Vibrations*, Edward Arnold Publishers Ltd, London, 1967, p. 98.
34 (*a*) H. J. Gericke, N. I. Barnard, E. Erasmus, J. C. Swarts, M. J. Cook and M. A. S. Aquino, *Inorg. Chim. Acta*, 2010, **363**, 2222; (*b*) D. H. Evans, K. M. O'Connell, R. A. Peterson and M. J. Kelly, *J. Chem. Educ.*, 1983, **60**, 290; (*c*) P. T. Kissinger and W. R. Heineman, *J. Chem. Educ.*, 1983, **60**, 702; (*d*) J. J. Van Benshoten, L. Y. Lewis and W. R. Heineman, *J. Chem. Educ.*, 1983, **60**, 772; (*e*) G. A. Mobbott, *J. Chem. Educ.*, 1983, **60**, 697.
35 (*a*) A. J. Fry, *Synthetic Organic Electrochemistry*, John Wiley and Sons, New York, 2nd edn, 1989, p. 208–232; (*b*) J. Volke and F. Liska, *Electrochemistry in Organic Synthesis*, Springer-Verlag, Berlin, 1994, p. 90.

36 M. L. Lage, M. J. Mancheño, R. Martínez-Álvarez, M. Gómez-Gallego, I. Fernández and M. A. Sierra, *Organometallics*, 2009, **28**, 2762.
37 See Computational Details.
38 This result is not surprising as the HOMO of the group 6 Fischer carbene complexes is located in the transition metal in most cases. See, for instance: (*a*) I. Fernández, M. A. Sierra and F. P. Cossío, *J. Org. Chem.*, 2006, **71**, 6178; (*b*) I. Fernández, M. A. Sierra and F. P. Cossío, *J. Org. Chem.*, 2008, **73**, 2083; (*c*) D. M. Andrada, A. M. Granados, M. Solà and I. Fernández, *Organometallics*, 2011, **30**, 466.
39 (*a*) C. Creutz and H. Taube, *J. Am. Chem. Soc.*, 1969, **91**, 3988; (*b*) M. J. Cook, I. Chambrier, G. White, E. Fourie and J. C. Swarts, *Dalton Trans.*, 2009, 1136; (*c*) N. Van Order, W. E. Geiger, T. E. Bitterwolf and A. L. Reingold, *J. Am. Chem. Soc.*, 1987, **109**, 5680; (*d*) D. T. Pierce and W. E. Geiger, *Inorg. Chem.*, 1994, **33**, 373; (*e*) E. Fourie, J. C. Swarts, I. Chambrier and M. J. Cook, *Dalton Trans.*, 2009, 1145; (*f*) W. E. Geiger, N. Van Order, D. T. Pierce, T. E. Bitterwolf, A. L. Reingold and N. D. Chasteen, *Organometallics*, 1991, **10**, 2403.
40 (*a*) K. C. Kemp, E. Fourie, J. Conradie and J. C. Swarts, *Organometallics*, 2008, **27**, 353; (*b*) W. C. Du Plessis, W. L. Davis, S. J. Cronje and J. C. Swarts, *Inorg. Chim. Acta*, 2001, **314**, 97.
41 The potentials of two closely-spaced redox events are very difficult to determine utilising voltammetric methods, see D. E. Richardson and H. Taube, *Inorg. Chem.*, 1981, **20**, 1287.

